Simulation of small-angle X-ray scattering from thylakoid membranes

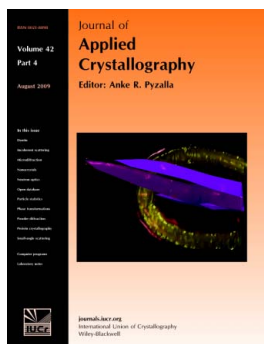## J. J. K. Kirkensgaard, J. K. Holm, J. K. Larsen and D. Posselt

Many research topics in condensed matter research, materials science and the life sciences make use of crystallographic methods to study crystalline and non-crystalline matter with neutrons, X-rays and electrons. Articles published in the *Journal of Applied Crystallography* focus on these methods and their use in identifying structural and diffusion-controlled phase transformations, structure–property relationships, structural changes of defects, interfaces and surfaces, *etc.* Developments of instrumentation and crystallographic apparatus, theory and interpretation, numerical analysis and other related subjects are also covered. The journal is the primary place where crystallographic computer program information is published.

Crystallography Journals Online is available from **journals.iucr.org**

Simulation of small-angle X-ray scattering from thylakoid membranes

J. J. K. Kirkensgaard,* J. K. Holm, J. K. Larsen and D. Posselt

Department of Science, Systems and Models, University of Roskilde, Denmark. Correspondence
e-mail: kirkensgaard@life.ku.dk

Small-angle X-ray scattering (SAXS) patterns are calculated from a three-dimensional model of photosynthetic thylakoid membranes. The intricate structure of the thylakoids is represented by sampling random 'electron density points' on geometric surfaces. The simulation setup works as a virtual instrument, allowing direct comparison with experimental data. The simulations qualitatively reproduce experimental data and thus clarify the structural origin of the scattering features. This is used to explain recent SAXS measurements and as a guideline for new experiments and future quantitative modeling. The setup has general applicability for model testing purposes when modeling scattering from membrane systems of complex geometries.

1. Introduction

In green plants, the process of photosynthesis takes place in small subcellular structures, named the chloroplasts. An extensive membrane system is located inside the chloroplast, known as the thylakoids. These membranes are crucial, as most of the protein systems that participate in the various stages of the photosynthetic processes are associated with this membrane system. The thylakoids display a unique organization on mesoscales (10–1000 Å), as they arrange into stacks of flattened vesicles termed grana stacks, interconnected by membrane sheets known as stroma lamellae. A key functional feature of this organization is to separate two aqueous domains, the lumen (inner domain) and the stroma (outer domain). This organization is illustrated two-dimensionally in Fig. 1 by a thin-section electron microscopy image of a single chloroplast. However, the precise three-dimensional organization is still a matter of debate (Shimoni *et al.*, 2005; Mustardy *et al.*, 2008; Brumfeld *et al.*, 2008; Garab & Mannella, 2008). The dominant three-dimensional model is based on the original work of Paolillo (1970) and describes the thylakoids as one large intricately folded structure with the stroma lamellae helically wound around the grana stacks (Mustardy & Garab, 2003). An idealized illustration of this organization is seen in Fig. 2. In the real biological system, the variability in sizes and distances is large and should be superimposed on the idealized model.

The stacked nature of the thylakoid system allows for a structural characterization in terms of the repeat distances of the grana and stroma lamellae domains, respectively, *i.e.* the system can be constructed by repeatedly placing unit cells on two lattices with respective lattice-point spacings corresponding to the repeat distances of the two different types of domains. A comparison of data reported in the literature (Paolillo *et al.*, 1969; Gunning & Steer, 1975; Brangeon &

Mustardy, 1979; Hodapp & Kreutz, 1980) reveals that the ratio of stroma lamellae to grana repeat distance varies between 2 and 3.3, the typical grana repeat distance being 160–240 Å. A possible distribution of distances within a grana unit cell as estimated from small-angle scattering would be a membrane thickness of ~40 Å, a lumen width of ~65 Å and an inter-thylakoid distance of ~20 Å, yielding a total of ~165 Å (each repeating unit cell contains two bilayers, see below). Inclination angles of the stroma lamellae between 12 and 26° and grana diameters of on average 25 times the repeat distance are found, corresponding to grana radii in the range 2000−3000 Å.

The overall purpose of our work is to determine the behavior of these distances as the thylakoids perform dyna-
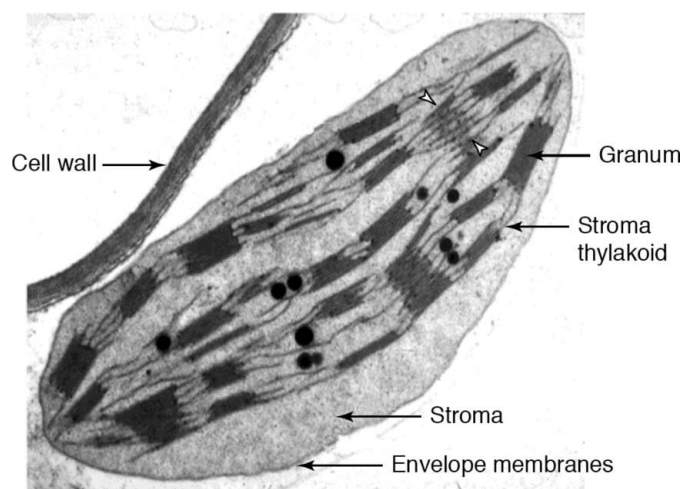
Figure 1
Electron microscopy image of a single chloroplast. We see the grana stacks connected by stroma lamellae. Notice the tilted stroma lamellae between the white arrows. Scale bar = 0.5 μm. Figure courtesy of A. L. Staehelin and R. Hallick.

649

mically, primarily during illumination but also upon changing other parameters like salt content, osmolarity and temperature. A structural effect of illumination was first reported by Murakami & Packer (1970) where it is shown that the thylakoid response to illumination is a contraction of the stack and a decrease in membrane spacing. The shrinkage is reversed when the membranes are subsequently permitted to rest in the dark. It is also demonstrated that increasing the osmotic pressure around the thylakoids leads to a contraction of the stack, similar to the contraction caused by illumination. It is further speculated that the stack radius and membrane thickness might be changing. Both the illumination and the osmotic pressure-induced shrinkage behavior is confirmed and further quantified in our recent work using small-angle neutron scattering (SANS) (Posselt *et al.*, 2009); however, mainly information on the overall stroma repeat distances was obtained, and not on the detailed unit-cell structure. The unit-cell behavior will be the focus of this paper.

The motivation for investigating the thylakoid system in terms of the unit-cell structure has arisen from performing identical experiments using small-angle X-ray scattering (SAXS) at higher q (probing shorter distances) where the situation turns out to be different: contrary to the SANS results, illumination now causes almost no difference in the scattering signal (not shown) while osmotic pressure variation does. In Fig. 3 a series of measurements are shown where the osmotic pressure on the membranes is changed by increasing the concentration of sorbitol in the outer medium. The two broad peaks are a characteristic scattering feature of the thylakoids, with the 0.4 *M* sorbitol suspension medium corresponding closest to the native state of the system. As can

be seen, the scattering signal is dramatically changed by the osmolarity variation, and it is natural to assume that these changes reflect both the structural changes in the system (which we know take place as is well documented both in the literature and from our SANS investigations) as well as the changes in contrast. The question remains, however, why no such changes are seen in the illumination SAXS experiments.

Here we will calculate the small-angle scattering from the three-dimensional structure shown in Fig. 2 in order to understand the structural origin of the scattering signal as it is manifested in recent SAXS experiments conducted in our laboratory. There are several reasons for this approach. Firstly, we wish to understand the above-mentioned discrepancies, and thus the present simulation setup is devised to elucidate the role of contrast and the characteristic length scales of the sample together with the range of length scales investigated in the SAXS experiments. Secondly, the simulations allow us to investigate a number of questions relevant for the formulation of an analytical mathematical model, which can be fitted directly to the experimental data to yield information on unit-cell parameters, not only overall repeat distances as in the SANS measurements. The formulation of such a quantitative model based on the above considerations and validated by the simulations will be presented elsewhere. Thirdly, the simulations can indicate whether the hitherto utilized SAXS setup suffers from any shortcomings in terms of actually retrieving the information we are aiming for and can thus be used as a guideline for future experiments. Lastly, the setup has general applicability for model testing purposes, especially with regard to membrane systems with complicated three-dimensional geometries.

2. Simulations

The simulation setup is designed as a 'virtual instrument' and basically consists of two steps. One is to model and represent whatever structure one wishes to investigate (in this case
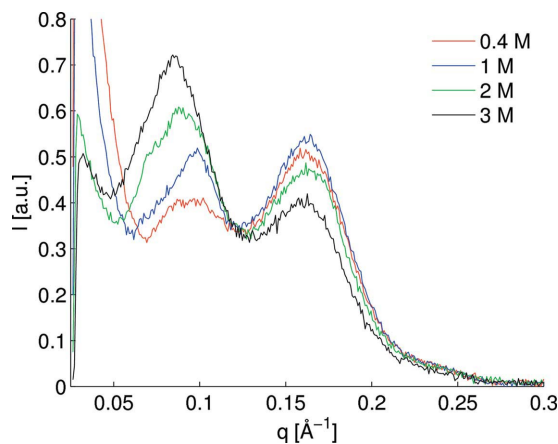

Figure 2
Three-dimensional model of the thylakoid membrane as suggested by Paolillo. Important structural parameters are the repeat distances of both the central grana stack and the surrounding helical stroma lamellae. Notice that at each level of flattened vesicles there appear a number of connection points around the stack, *i.e.* it is not a single sheet winding around the stack. Figure courtesy of B. Gunning (http://www.plantcellbiologyondvd.com).

Figure 3
Experimental SAXS data from isolated thylakoid membranes. The legend indicates the sorbitol concentration of the surrounding medium. Upon increasing the osmolarity the right peak stays fixed in position but decreases in amplitude, while the left peak grows and shifts to lower q.

thylakoid membranes) as a discrete three-dimensional electron density distribution; the other is to calculate the scattering from this structure and process it to compare with real experiments. The simulation setup is thus designed to mimic a particular experimental setup. In the present case, the SAXS experiments are performed using a slit-collimated Kratky camera; however, the specific simulation setup is easily modified to represent any other scattering setup. Two pieces of experimental information are especially relevant for the present simulations: First, the slit collimation of the Kratky camera introduces a smearing of the scattering signal, which must be accounted for when comparing simulation results with experiments (see Appendix A). Second, the thylakoids are aligned in a magnetic field, which results in non-isotropic scattering. The alignment increases the intensity on the Kratky camera one-dimensional detector, and when using a two-dimensional detector (as in our SANS measurements) the changes in the characteristic scattering features can be followed visually 'online' when all scattering intensity is collected in two broad and intense spots.

2.1. Calculating the scattering

Historically, a number of approaches have been presented to simulate small-angle scattering spectra, most of which focus on orientationally averaged samples (Hansen, 1990; Schmidt-Rohr, 2007) and a few on oriented samples (McAlister & Grady, 1998; Förster *et al.*, 2005). Owing to the magnetic alignment of the thylakoids, we cannot take advantage of various approaches that implicitly incorporate an orientational averaging (for example, the Debye equation), so instead we take as our starting point the fundamental equation

$$A(\mathbf{q}) = \sum_{j=1}^{N} b_j \exp(i\mathbf{q} \cdot \mathbf{r}_j) \qquad (1)$$

for calculating the scattering amplitude $A(\mathbf{q})$. Here $\mathbf{q}$ is the scattering vector with magnitude $q = 4\pi \sin(\theta)/\lambda$, where λ is the radiation wavelength and θ is half the scattering angle, N is the number of scattering objects, and b_j and $\mathbf{r}_j$ are the scattering length and spatial position of the jth scattering object, respectively. A 'virtual detector' is overlaid with a grid and the scattering amplitude is calculated for each grid point, corresponding to a particular $\mathbf{q}$ vector. The intensity is then obtained directly from equation (1) as $I(\mathbf{q}) = |A(\mathbf{q})|^2$. The resolution of the grid is chosen sufficiently high to ensure that information is not lost (tested, not shown). In practice this means 1000 partitions per centimetre detection length, which corresponds to each grid point representing a $10 \times 10\,\mu\text{m}$ pixel. The detection area also matches the Kratky camera detector (6×1 cm) and is projected onto the measuring axis of the detector. Finally, this one-dimensional scattering curve is binned into channels containing six grid points to match the Kratky camera channel width of $\sim$60 µm and smeared to compare with experimental data as outlined in Appendix A. Although the above approach is 'brute force' and rather time-consuming, the calculations are still manageable on a standard

desktop computer (a couple of hours for a typical calculation of one unit cell).

2.2. Modeling the structure

In a real system, the membranes building the thylakoid structure consist of a mixture of lipids in which the various photosynthetic proteins, pigments and protein complexes are embedded. In the model, we average over the structure laterally, thus neglecting any lateral organization with contrast variation giving rise to small-angle scattering. For convenience, the bilayer nomenclature with a hydrophiphilic 'head group' and hydrophopic 'tail group' region is used throughout, and the high protein content is thus only reflected in the average contrast of the system, not in any lateral contrast variation.

The virtual sample aims to represent the structure in Fig. 2, and thus consists of two parts: an inner cylindrical stack of double lipid bilayers surrounded by helical sheets of double lipid bilayers (both with proteins embedded, see above). In the calculations we ignore the actual connection points between the two domains, but for convenience we refer to them below in the model construction. The usual approach in data treatment of stacked membrane systems is to model a one-dimensional electron density profile along the direction perpendicular to the membrane plane with densities taken relative to the surrounding medium (Pabst *et al.*, 2003). We will also adopt this approach for both the grana stack and the stroma lamellae along the direction of the membrane normal. In Fig. 4 a detailed view of the distances and parameters involved in this approach is shown (see caption for details; the physical quantities described by the parameters are listed in Table 1). The electron density profile in the perpendicular direction is represented as a sum of six Gaussians (representing either hydrophilic or hydrophobic groups), while a uniform lateral electron density is assumed as explained above. Such a one-dimensional model can be analytically Fourier transformed and we will compare the three-dimensional simulations with this when relevant. This calculation is outlined in Appendix B.
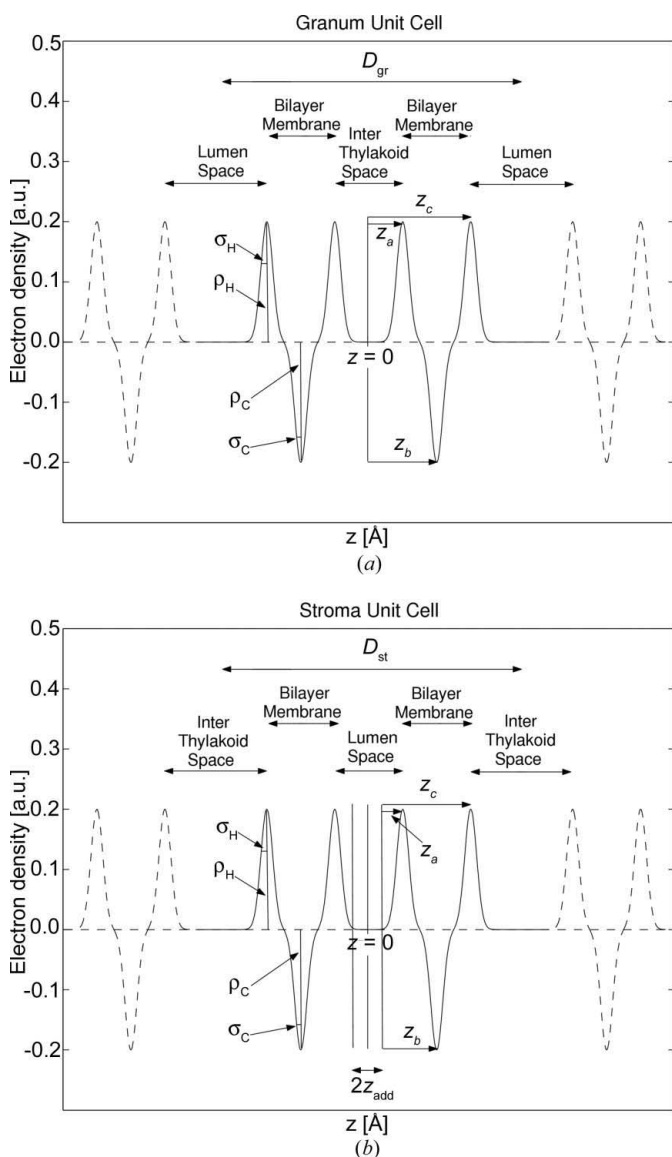
To build the actual structure shown in Fig. 2 we sample points randomly from two different surfaces: a disc for the grana stack and a helicoid for the stroma lamellae. These 'electron density points' will be assigned to either a hydrophilic Gaussian or a hydrophobic Gaussian corresponding to Fig. 4. All points in such a group will share the same electron density value (ρ_H or ρ_C, respectively); however, the Gaussian electron density distribution is ensured through the distribution of points along the normal to the grana and stroma lamellae stack.

The grana stack is built from unit cells, each consisting of six discs of points with four representing hydrophilic groups and two representing hydrophobic groups, as exemplified in Fig. 5. The points are distributed randomly: uniformly in the plane of the discs and following a Gaussian distribution along the plane normal corresponding to the parameters in Fig. 4. The various

Table 1
Physical parameters derived from the model parameters (compare with Fig. 4).

Derived parameter	Grana stack	Stroma lamellae
Membrane thickness	$z_c - z_a + \sigma_H$	$z_c - z_a + \sigma_H$
Inter-thylakoid distance	$2z_a - \sigma_H$	$D_s - 2z_{add} - 2z_c - \sigma_H$
Lumen distance	$D_g - 2z_c - \sigma_H$	$2z_a + 2z_{add} - \sigma_H$
Repeat distance	D_g	D_s

distances will thus be reflected in the relative positions of the centers of gravity of the sampled points of each disc.
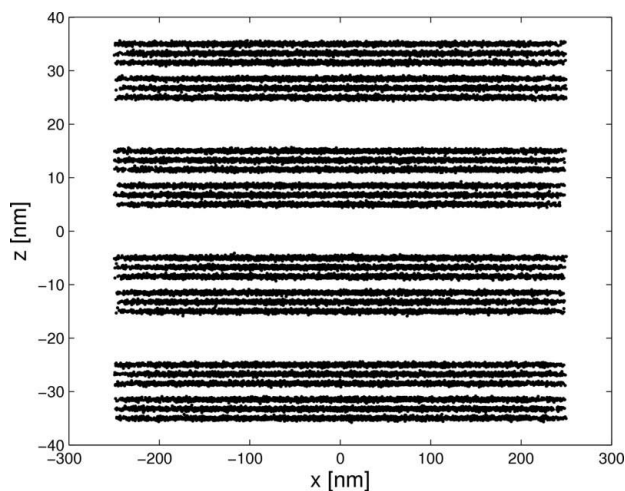
To construct the helical stroma domain, we will distribute points on a helicoid wrapped around the center cylinder of the grana stack. The helicoid is parametrized as

$$\mathbf{h}(s, \varphi) = (s \cos \varphi, s \sin \varphi, \lambda_p \varphi), \quad (2)$$

where s and φ are radial and angular azimuthal coordinates, respectively, and λ_p is the pitch constant. The radial coordinate is restricted to an interval $[R_{inner}, R_{outer}]$, where R_{inner} is the grana stack radius. As with the discs, the points are uniformly distributed radially and Gaussian perpendicular to the membrane surface.

Since the parametrization in equation (2) only produces one helicoid sheet we generate a helicoid for each connection point around the grana stack (see Fig. 2). This is easily achieved by rotating M/m of the M randomly generated points by an angle $2\pi j/m$, where m is the number of connections and $j = 1, 2, \ldots, m$. In Fig. 6 this is illustrated for eight connection points, which will be our choice throughout this investigation.

As with the grana stack, we want to make six sheets to represent the 'head' groups and 'tails', respectively. This is again achieved by making displacements perpendicular to the surface; however, this direction is not constant on the helicoid. To determine the perpendicular direction everywhere on the helicoid we compute the standard unit normal vector, defined as

Figure 4
Electron density profiles of the two unit cells. (a) Granum unit cell. (b) Stroma lamellae unit cell. The direction of the z axis is along the normal to the membrane plane. The physical quantities described by the parameters are listed in Table 1. Note that the two unit cells are centered differently. This choice reflects an underlying assumption about the flexibility characteristics of the two stacks. This assumption is based on biological evidence indicating that the grana stack inter-thylakoid distance and the stroma lamellae lumen distance have the smallest distance fluctuations (Holm, 2004). In a modeling context, this means that the assumed larger distance fluctuations of the grana lumen and stroma lamellae inter-thylakoid compartment will be described by the relative positions of the unit cells, *i.e.* as a structure factor disorder.

Figure 5
Grana stack with four unit cells viewed in the xz plane (the xy plane would show a uniform disc). Each triplet of discs represent a bilayer with two head group regions surrounding a tail region. The repeat distance is 200 Å, $z_a = 15$ Å, $z_b = 32.5$ Å, $z_c = 50$ Å, $\sigma_H = \sigma_C = 2$ Å and the radius is 2500 Å. From Table 1 this corresponds to a membrane thickness of 37 Å, an inter-thylakoid distance of 28 Å and a lumen distance of 98 Å. Note that the Gaussian distribution of points along the stack normal for graphical reasons is represented by bands of black points separated by white areas. If the spread of the Gaussians were larger, it would be impossible to distinguish neighboring Gaussians.

$$\mathbf{N} = \frac{\mathbf{h}_s \times \mathbf{h}_\varphi}{\|\mathbf{h}_s \times \mathbf{h}_\varphi\|}, \tag{3}$$

where the subscript denotes partial differentiation with respect to the coordinate given. We find that

$$\mathbf{N} = (\lambda_p^2 + s^2)^{-1/2}(-\lambda_p \sin\varphi, \lambda_p \cos\varphi, -s). \tag{4}$$

The displacements needed to build the helical structure and the spread of the associated Gaussians will thus be made along the direction of $\mathbf{N}$. An example is illustrated in Fig. 7 for an $m = 3$ stroma lamellae unit cell.

Basically, this constitutes the sample generation procedure. Again there is an issue of resolution related to how many electron density points are needed to represent the structure adequately. This is determined by simulation; when the scattering curve normalized with respect to the number of electron density points does not change upon adding more points, the
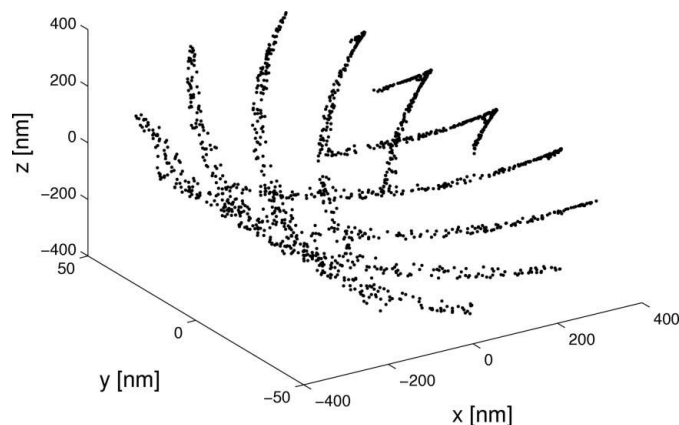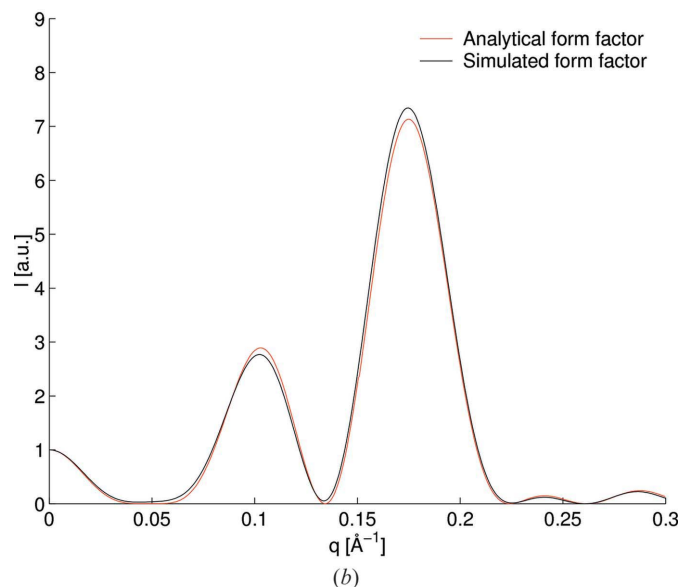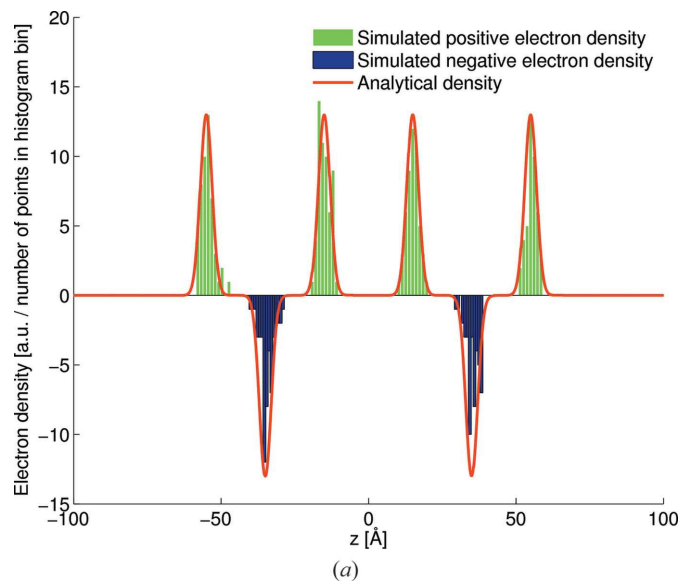

Figure 6
Generation of helical stroma lamellae sheets with eight connection points. Repeat distance is fixed at 300 Å. The outer radius is artificially small here for visualization purposes.
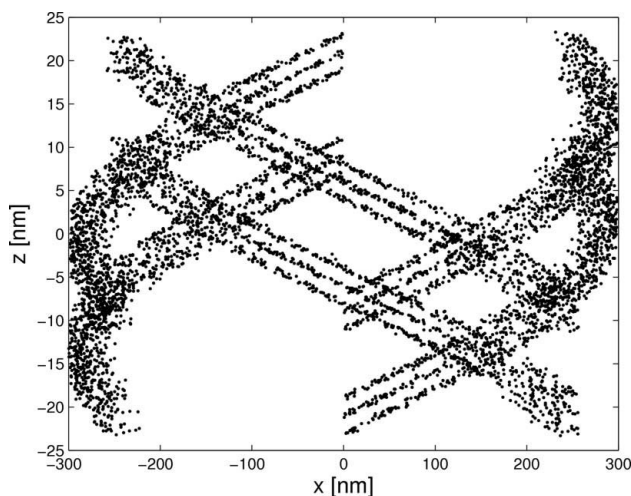
Figure 7
Stroma unit cell, xz projection. Only an $m = 3$ connection point unit cell is shown for visual clarity; all simulations are with $m = 8$. Parameters: $z_a + z_{add} = 40$ Å, $z_c + z_{add} = 80$ Å, z_b centered between z_a and z_c, $\sigma_H = \sigma_C = 2$ Å, $R_{inner} = 2500$ Å and $R_{outer} = 3000$ Å. From Table 1 this corresponds to a membrane thickness of 40 Å, an inter-thylakoid distance of 140 Å and a lumen distance of 80 Å.

structure is assumed to be sufficiently well represented. The point densities of the two domains are set to be equal to ensure that the scattering signal is completely controlled by the electron densities specified. The implementation of this density constraint is outlined in Appendix C. Furthermore, here we have only shown the two domains separately, but since the scattering amplitude in equation (1) is additive, we are free to simulate the two domains separately or combined. This way we can clarify which part of the structure gives rise to which features of the scattering and investigate the effect of interference between the two domains, when calculating the

Figure 8
Comparing the analytical and simulated form factors of a one-dimensional grana unit cell by simulating with a radius close to zero, here 1 Å. The analytical electron density profiles are obtained by summing the Fourier transform of six Gaussians with the relevant parameters (see Appendix B). All simulated Gaussians contain 100 particles each. (a) Double bilayer unit cell with four Gaussians built from electrons with scattering length +1, and two Gaussians with scattering length −1. The histograms show the spatial sampling of points, which is Gaussian. (b) Form factors corresponding to (a).

electronic reprint

scattering intensity as the absolute square of the amplitude. We will utilize both options in the following.

3. Results and discussion

In this section we will first present simulation results from the individual domains (grana and stroma lamellae, respectively) and discuss these in relation to the analytical one-dimensional profile model. We proceed to simulate the scattering from the combined unit cell and discuss both the unsmeared and smeared simulation data as well as some of the assumptions made in the calculations. Finally we set up a realistic contrast variation series to mimic the osmolarity measurements and discuss the results in relation to the experimental data presented previously in Fig. 3.

3.1. Grana unit cell

First we will investigate the changes in the scattering pattern when going from one to three dimensions simply by looking at the effect of increasing the radius of the grana in the simulations. In Fig. 8 we see that the simulation of a single grana unit cell with a radius close to zero (1 Å) is in good agreement with the analytical form factor from the one-dimensional electron density profile. It is not surprising that there is good correspondence between the analytical model and the simulation result when the simulation is for a virtual one-dimensional grana unit cell. For the opposite limit of large grana stack radii it is also *a priori* expected that the representation of scattering from a thin disc by a one-dimensional profile multiplied by the so-called Lorentz factor is valid when the lateral dimensions are much larger than the thickness, as first derived by Porod (Glatter & Kratky, 1982). In Fig. 9 we show the result of increasing the radius, where the criterion of large lateral dimensions is expected to be met for $R_{inner} = 2500$ Å, and we compare the simulation result with the 'bare' one-dimensional
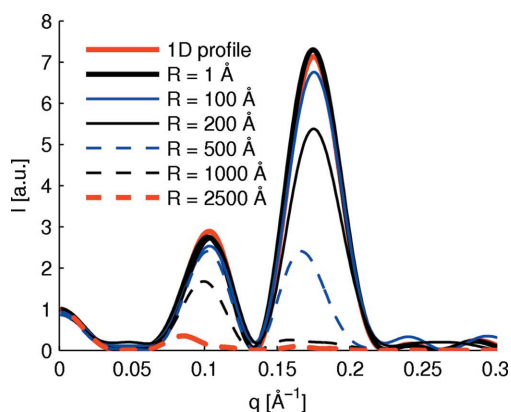
Figure 9
Variation of the grana radius. As the radius is increased the scaling crossovers move towards lower q progressively scaling the scattering curves more and more [compare with equation (5)]. At radii up to 500 Å mainly the right peak is affected, but when reaching 1000 Å also the second peak is altered, meaning that the regime crossover is now moving through this peak. At a radius of 2500 Å the whole curve is in the q^{-4} regime.

model. As can be seen, as the radius is increased, the agreement between the one-dimensional model and the simulated scattering curve gets progressively worse.

We conclude that in order to take into account that the large-radii simulations deviate substantially from the analytical one-dimensional model two issues should be addressed; first, the different scaling regimes of the scattering curve should be considered, and second, the effect of the radius should be explicitly included in the analytical model in three dimensions. Such a detailed modeling of the effect of the radius will not be considered further here since it does not influence the conclusions based on the simulations. As it turns out the main effect is in fact the first issue. If we limit the discussion to a thin disc, it has been shown that with increasing q the scaling of the orientationally averaged intensity for an isotropic system goes through a series of exponents (Shibayama *et al.*, 1989), as

$$I(q) \propto \begin{cases} q^0 & \text{if } q < q_R^*, \\ q^{-2} & \text{if } q_R^* < q < q_L^*, \\ q^{-4} & \text{if } q_L^* < q. \end{cases} \quad (5)$$

q_R^* and q_L^* are the scattering regime crossover positions related to the characteristic distances of the system, here given as approximately the inverse of the disc radius R and thickness L, respectively. This behavior also applies for an oriented system; however, the positions of the crossovers become dependent on the degree of orientation (Shibayama *et al.*, 1989). In practice this dependence is described by new 'effective' distances, which in our case with a very high degree of orientation and measuring along the cylinder axis means that $q_R^* \ll q_L^* \simeq 1/100$ Å $= 0.01$ Å^{-1}, which is lower than the experimental q range (here 100 Å is chosen as a representative lower bound of a double bilayer unit cell). In other words, the scattering from the grana unit cell disc in the investigated q range is all located in the q^{-4} (Porod) regime and so the one-dimensional model should be scaled accordingly to be in agreement with the three-dimensional simulations. This is illustrated in Fig. 10 for the $R_{inner} = 2500$ Å simulation from Fig. 9 for three different membrane thicknesses. The overall peak amplitudes are now in reasonable agreement, although the simulation profiles experience some undulations and shifts not seen in the one-dimensional model; we ascribe these discrepancies to the radius effect mentioned above, which is not accounted for. In general, the whole issue of the scaling regimes is highly dependent on the combination of the geometric dimensions and degree of orientation of the scattering object and the q range in question [for example, for a thin rod, the middle regime in equation (5) scales as q^{-1} and the characteristic distances change order (Shibayama *et al.*, 1989)]. This will also be evident below, since these problems are not an issue with the helical stroma lamellae domain where the unit cell is a cylinder with a hole in the middle. Based on the experimental numbers mentioned in the introduction we will keep the radius of the grana domain constant at 2500 Å from here on.

3.2. Stroma lamellae unit cell

We now turn to simulating the stroma lamellae domain, represented by helical sheets of double bilayers as explained previously. As also stated we will limit the simulations to $m = 8$ sheets, and we will maintain the inner radius at $R_{inner} = 2500$ Å and set the outer radius of the sheets to twice that value, *i.e.* $R_{outer} = 5000$ Å. In reality the number of connection points varies, so $m = 8$ represents an average number; however, changing m makes no difference in the shape of the scattering signal (although the whole curve is scaled since more points are used for higher m), except for a minor symmetry-related difference between even and uneven m (not shown). We will return to the effect of changing the outer radius of the stroma lamellae below and show that 5000 Å is a reasonable choice. In Fig. 11 we see that the
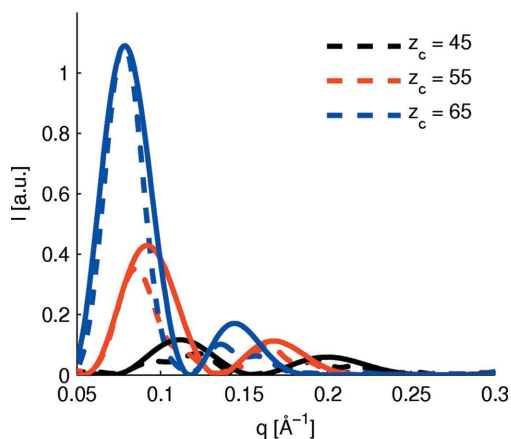
Figure 10
Scaling the one-dimensional model with q^{-4} ensures that the peak amplitudes are in agreement with the three-dimensional simulations of the 2500 Å radius grana stack from Fig. 9. The dashed red curves in the two figures are the same. Full lines are q^{-4}-scaled one-dimensional model form factors and dashed lines are corresponding simulation results. The scaling is illustrated here by changing the membrane thickness (changing z_c).
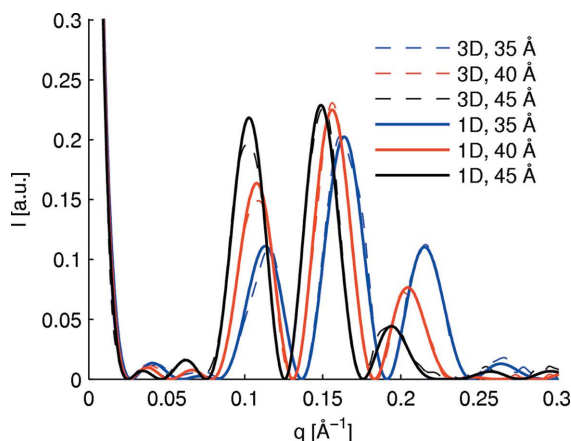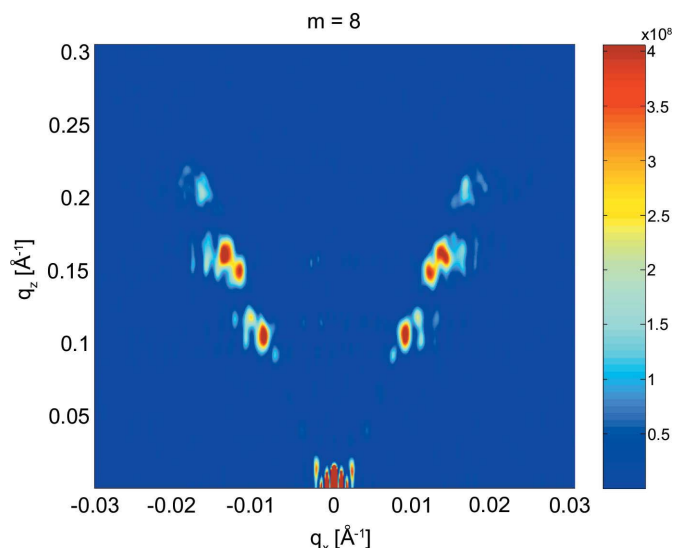

Figure 11
Comparing stroma lamellae three-dimensional simulations and the one-dimensional profile model scaled by q^{-1}, exemplified by changing the stroma lamellae membrane thickness (indicated in the figure legend). Simulated results with lumen distance = 80 Å, tails centered in membrane and $\sigma_H = \sigma_C = 2$ Å.

simulations of the stroma lamellae are in excellent agreement with the one-dimensional model scaled by q^{-1}. This conclusion is valid for all parameters varied in the investigation. The result is what is expected from an oriented system when including the standard Lorentz correction (Crist & Morosoff, 1973; Nagle & Tristram-Nagle, 2000). Normally when applying a one-dimensional-profile model to an isotropic assembly of stacked systems, one would employ the Lorentz correction factor q^{-2} to account for the isotropically distributed intensity. Upon orientation, this correction reduces to q^{-1}. As already mentioned above, the scaling behavior seen with the grana is not seen with the stroma lamellae, which is most likely simply a result of the differences in geometry, orientation and length scales between the two domains. Another aspect of these differences is seen in Fig. 12 where a simulated two-dimensional detector image is shown, illustrating the effect of the inclination angle due to the helical nature of the stroma lamellae.

3.3. Complete thylakoid unit cell

In Fig. 13(*a*) we see a typical full simulation (one unit cell) of the combined grana stack and stroma lamellae, together with separate simulations of the individual domains and the sum of these individual non-interfering contributions. Several conclusions can be drawn from this result. First, it is evident that the overall signal is dominated by the stroma lamellae, not the central grana stack. This is obvious in light of the different scaling properties discussed above but was not the initial expectation. Second, we can see that simply adding the contributions of the individual domains is a fairly good approximation to the full interfering signal. This is very important for modeling purposes, since this allows the two domains to be modeled separately. Furthermore, this allows us to draw conclusions directly from simulations of individual
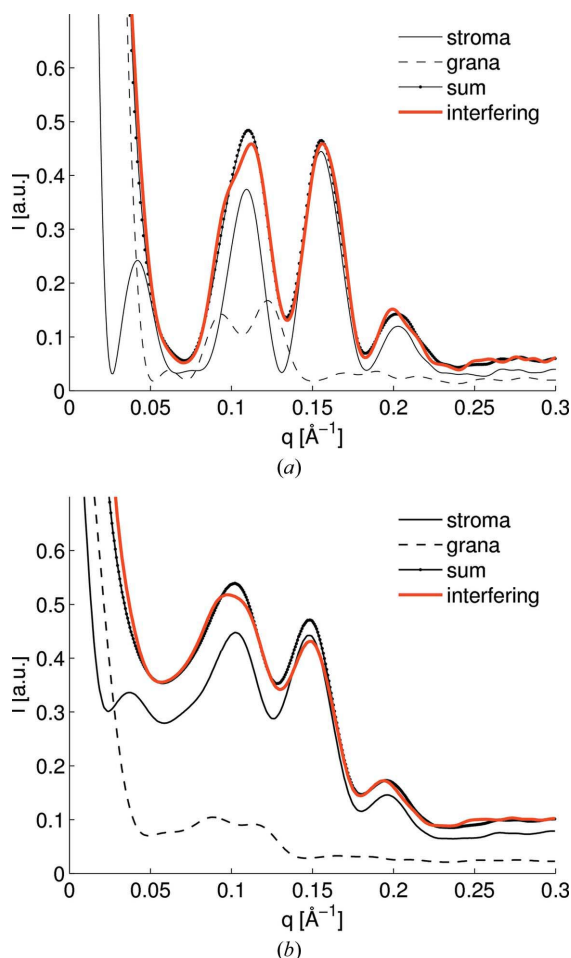

Figure 12
Two-dimensional detector image of the 40 Å membrane thickness sample from Fig. 11. The inclination angle of the helical stroma lamellae gives rise to a characteristic cross pattern (only half the detector is shown).

J. J. K. Kirkensgaard *et al.* • Simulation of SAXS from thylakoids

domains without the need for performing the computationally much heavier combined simulations.

Looking at Fig. 13(b) we see the same simulation results smeared with the experimental resolution function. It is evident that the simulation captures the main features of the data as it very closely resembles the 2 M curve from Fig. 3. One difference is the small peak around $q = 0.2 \, \text{Å}^{-1}$; however, a small bump is in fact seen in several data sets (not shown), although less pronounced, which we ascribe to an averaging effect (the simulation is of one structure with well defined parameters, which is of course not the case in the real system). We also see that the domination of the stroma lamellae signal is enhanced by the smearing effect.

The domination of the stroma lamellae signal is strongly coupled to the ratio of simulated points between the grana stack and the stroma lamellae, thus returning to the question of which value to use for the outer radius of the stroma lamellae. In Fig. 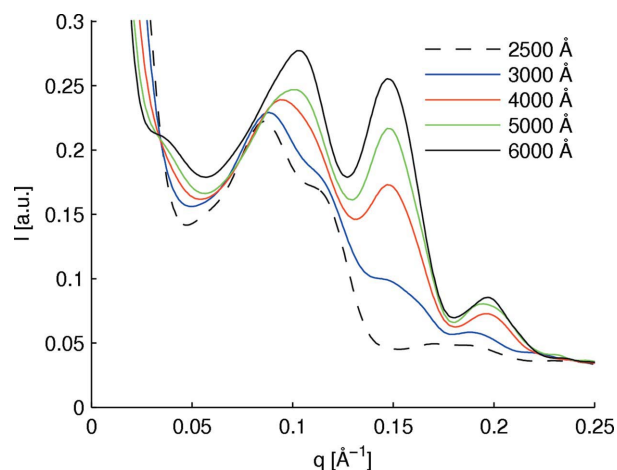14 we see a number of simulations with a fixed-radius central grana stack and an increasing stroma lamellae radius. Fig. 14 shows that the choice of outer radius is crucial for the final result. Comparing with the experimental data it is clear that setting the outer radius too low does not produce scattering profiles that are compatible with the experimental data. This validates the choice of radius employed here and in fact is a strong indication that the modeling of this system requires the contribution from this domain. As previously mentioned, the three-dimensional stroma lamellae structure is excellently represented by the one-dimensional model scaled properly. As a further substantiation of this result the pure stroma lamellae radius variation profiles are practically identical when normalized with the number of simulated points (not shown). Thus, the variation of the stroma lamellae outer radius corresponds to scaling the contribution from this domain relative to the grana stack contribution.

3.4. Realistic contrast variation series

In Fig. 15 (a) we see an indication of the range of relevant electron densities in the thylakoid membrane. To produce realistic contrast variation simulations we will make a simple model based on these numbers, as well as on biological knowledge of the differences between the protein content of the grana stack and the stroma lamellae. It is well established that the grana stack is more crowded with proteins than the stroma lamellae (Kirchhoff et al., 2002). In the following we will investigate a realistic system with a 70/30% protein/lipid content in the grana stack and a 40/60% protein/lipid content in the stroma lamellae and vary the electron density of the surrounding medium, i.e. mimicking the changing of the contrast when altering the osmolarity in the experiments. To do this we set the head group electron density to 0.6, the tail region to 0.32, proteins to 0.43 and the low/medium/high osmolarity solution levels to 0.35/0.4/0.45, respectively. The

Figure 13
Thylakoid simulation of one unit cell. (a) Unsmeared simulation results of individual structures, sum of these structures and the full sample. (b) As in (a), but profiles have been smeared with the Kratky camera resolution function. Grana parameters: $z_a = 10$ Å, $z_c = 50$ Å, $z_b = z_a + (z_c - z_a)/2$ (centered), $R_{inner} = 2500$ Å, $\rho_H = 1$, $\rho_C = -0.3$ and $\sigma_H = \sigma_C = 5$ Å. Stroma lamellae parameters: $z_a + z_{add} = 40$ Å, $z_c + z_{add} = 80$ Å, z_b centered, $R_{outer} = 5000$ Å, $\rho_H = 1$, $\rho_C = -0.5$ and $\sigma_H = \sigma_C = 5$ Å.
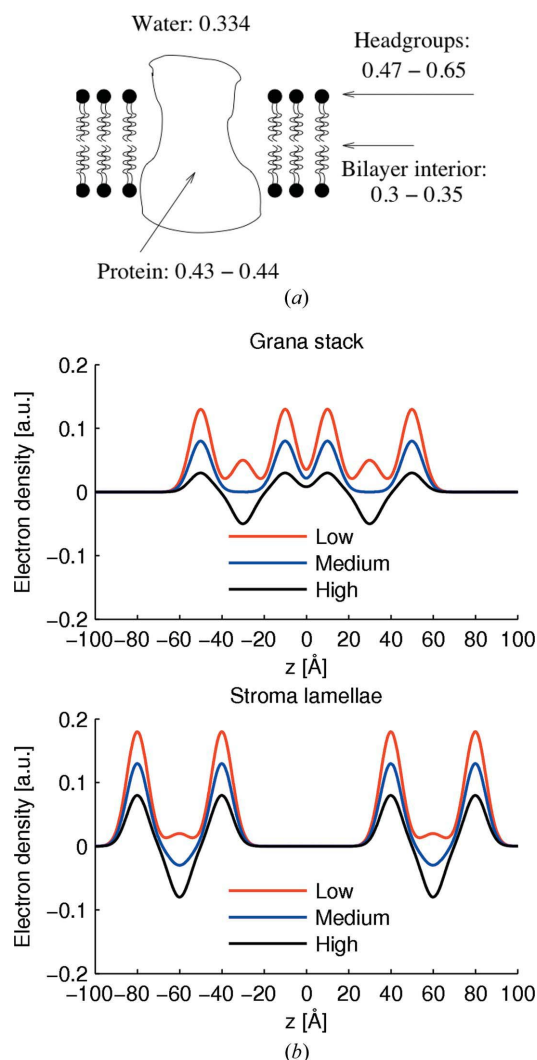

Figure 14
Simulating a full thylakoid unit cell while varying the outer radius of the stroma lamellae and keeping the grana stack radius fixed. Comparing with the experimental data shows that an outer radius of 4000–6000 Å is necessary to capture the data. The simulation data are normalized to $q = 0$.

last three numbers are rough calculations assuming 0.4, 1 and 4 *M* sorbitol content in an aqueous phase with a water electron density of 0.334 (using the mass densities and molar masses). The resulting electron density profiles from such a model are shown in Fig. 15(*b*). Notice that the different protein contents in the two membrane domains lead to separate contrast matching of the interior region in the two domains.

The results from these contrast simulations are shown in Fig. 16. It is immediately clear that the simulations qualitatively reproduce the osmolarity measurements in terms of the behavior of the two main peaks (compare with Fig. 3). Since we have only simulated one unit cell throughout these investigations, the fact that the data are so well captured by the
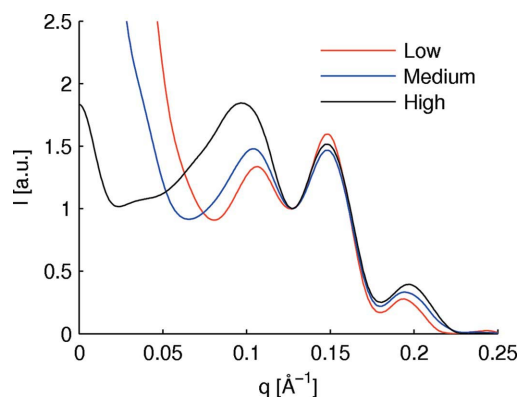
simulations indicates that the signal is primarily form factor scattering. In other words, the structural changes that we know take place when increasing the osmolarity are only weakly manifested in this *q* range. This most likely also can explain why only very small changes are seen in the scattering upon illumination, since in this case the structural changes are not accompanied by huge contrast effects. We have performed simulations with two or three unit cells stacked, which give rise to distinct Bragg peaks in the simulated spectrum (not shown). Such peaks are not observed in the experimental data (or only occasionally as very weak shoulders in the scattering curve). However, the 'missing' structure factor peaks in the experimental data can also just be due to the presence of a high degree of disorder in the biological sample. Such disorder is so far not explicitly included in the simulations.

4. Conclusions and outlook

A straightforward simulation setup has been presented, combining a brute-force calculation of the scattering amplitude with a Monte Carlo generation of the samples to be investigated. On the basis of this simulation, the scattering curve from a three-dimensional model of thylakoid membranes has been calculated. The simulations indicate that in the investigated *q* range the observed SAXS scattering curve is pure form factor scattering, and that contrast effects caused by the addition of sorbitol to the media surrounding the thylakoids play an important role in explaining the significant osmotically induced changes seen in the SAXS experiments. To obtain information on distances within the unit cell, additional modeling is needed in order to clarify the effect of the three-dimensional geometry of the system. It might be possible to reliably extract both grana and stroma lamellae unit-cell parameters if measuring on a setup with point collimation, since the slit collimation smearing effect contributes to enhancing the domination of the stroma lamellae scattering.

In respect to the formulation of a fitting model four things stand out as important lessons from the simulations. First, the

Figure 15
(*a*) Experimental electron densities in units of e Å⁻³ (from Blaurock, 1982). Setting the head group electron density to 0.6, the tail region to 0.32, proteins to 0.43 and the low/medium/high osmolarity solution levels to 0.35/0.4/0.45, respectively, leads to the contrast variation series shown below when employing the model of 70/30–40/60% protein/lipid content in the grana stack and stroma lamellae, respectively. (*b*) Contrast variation series corresponding to the simulations in Fig. 16. The osmolarity levels are indicated in the figures. Notice that the bilayer interior electron density is actually higher than the surrounding medium for low osmolarity owing to the protein content.

Figure 16
Full thylakoid unit-cell contrast simulation of the electron density profiles shown in Fig. 15. The relative peak behavior is seen to closely resemble the experimental data from Fig. 3. The data have been normalized to coincide at the minimum around *q* = 0.13.

scattering can approximately be described as a sum of two terms, one from the grana stack and one from the stroma lamellae, ignoring the interference effect between the two which is mainly important at low q ($q < 0.03$ Å^{-1}). Second, an important insight resulting from our simulations is the different scaling behavior of the grana and stroma lamellae contribution to the scattering, which should be considered in the modeling. Third, it is shown to be possible to represent the stroma lamellae domain by a one-dimensional Gaussian electron density profile provided the correct geometrical scaling factor is accounted for. Finally, the restricted lateral dimensions of the system need to be considered explicitly when modeling the scattering curves.

It should be emphasized that the thylakoid membrane system investigated is a full biological system and as such is subject to a large variability in the exact value of parameters describing the system (number of layers in a grana stack, grana and stroma dimensions *etc.*). In addition, we average over the lateral electron density, *i.e.* the presence of protein complexes is not explicitly taken into account. In spite of these complex issues, our data show that important information can be obtained from a scattering experiment averaging over the sample and the qualitative simulation tool presented in this work constitutes an important guide in interpreting the results. More generally, the setup should be considered a strong alternative as a model testing aid for systems with complicated geometries, especially membranes or other systems with varying electron density where one invokes dimension-reducing assumptions in the data analysis.

APPENDIX *A*
Experimental details and numerical smearing

Thylakoid membranes were isolated from systematically grown pea plants following the procedure outlined in detail by Posselt *et al.* (2009). Basically, the outer chloroplast membrane was removed by osmotic shock, and the native stroma solution was replaced by a controlled environment surrounding the thylakoids.

Measurements were made on a modified slit-collimated Kratky camera allowing for online illumination of the sample. The source radiation was delivered by a copper anode with $K\alpha$ radiation at a wavelength of 1.54 Å, which was further filtered by electronic energy discrimination of the detected photons. The scattering was detected on a one-dimensional gas-filled position-sensitive detector with a sample–detector distance of 26.7 cm. The covered q range in these investigations was 0.04–0.3 Å^{-1}. The scattering from the thylakoids was featureless for $q > 0.3$ Å^{-1}. The thylakoids were aligned in a 0.4 T magnetic field supplied by a set of permanent magnets around the sample. The cause of the alignment was a diamagnetic anisotropy in some of the membrane-bound proteins (Heinen *et al.*, 2004). The total sum of these rather small individual magnetic moments provides a total moment sufficient to align the molecules along an axis perpendicular to the membrane plane.

For more details on slit-collimation see Kratky & Stabinger (1984). In short, the incoming radiation is not point-like but has the shape of a line. This means that a photon detected at a specific position on the detector could have originated from any place along the line-shaped beam. This introduces what is known as a smearing effect, which has to be accounted for in the data analysis (we ignore the minor smearing contributions from the width and wavelength spread of the beam). Along the one-dimensional detector axis (y axis) each detection position corresponds to a range of q values given by

$$q = (x^2 + y^2)^{1/2}, \qquad (6)$$

where x is the coordinate along the line-shaped beam. The smeared intensity is given by

$$I_{\text{smear}}(y) = \int I_{\text{sim}}[(x^2 + y^2)^{1/2}] P(x) \, \mathrm{d}x, \qquad (7)$$

where $P(x)$ is the measured beam profile in the x direction. To perform the smearing of the simulated scattering profiles this equation is integrated numerically. Since there is not an exact correspondence between the simulated and measured q values we simply sample the simulated I_{sim} corresponding to the q_{sim} value closest to the q value in the integral, which causes no detectable difference in the result.

APPENDIX *B*
One-dimensional electron density profile

We will only calculate the one-dimensional profile for the grana stack; that for the stroma lamellae is the same except that the relevant parameters have to be changed according to Fig. 4. The calculation follows the approach of Wiener *et al.* (1989), ascribing to each unit cell an electron density profile based on Gaussian approximations of the lipid head and tail groups, respectively. Referring again to Fig. 4, the electron density profile for the granum unit cell is

$$\begin{aligned}
\rho_G(z) = \rho_{\text{H}} &\left\{ \exp\left[-\frac{(z - z_a)^2}{2\sigma_{\text{H}}^2} \right] + \exp\left[-\frac{(z + z_a)^2}{2\sigma_{\text{H}}^2} \right] \right\} \\
+ \rho_{\text{C}} &\left\{ \exp\left[-\frac{(z - z_b)^2}{2\sigma_{\text{C}}^2} \right] + \exp\left[-\frac{(z + z_b)^2}{2\sigma_{\text{C}}^2} \right] \right\} \\
+ \rho_{\text{H}} &\left\{ \exp\left[-\frac{(z - z_c)^2}{2\sigma_{\text{H}}^2} \right] + \exp\left[-\frac{(z + z_c)^2}{2\sigma_{\text{H}}^2} \right] \right\}, \quad (8)
\end{aligned}$$

where ρ_{H} and ρ_{C} denote the average electron density amplitude of the lipid head groups and the methyl groups of the bilayer interior, both relative to the suspending medium, and σ_{H} and σ_{C} the standard deviations of the Gaussians associated therewith. As can be seen, the electron density profile is symmetric around the center of the unit cell. From this center z_a and z_c denote the distances to the lipid head groups and z_b the distance to the minimum of the methyl group electron density, which is not necessarily at the bilayer center. The actual physical parameters derived from the model parameters are listed in Table 1. The evaluation of the model form factor can be carried out analytically. Each form factor receives contributions from three different Gaussians at three

different distances from the center of the unit cell, each counting twice as the cell is symmetric, *i.e.*

$$F(q) = 2F_a(q) + 2F_b(q) + 2F_c(q). \tag{9}$$

For the granum unit cell

$$F_b(q) = (2\pi)^{1/2} \sigma_C \rho_C \exp(-\sigma_C^2 q^2/2) \cos(qz_b) \tag{10}$$

and

$$F_i(q) = (2\pi)^{1/2} \sigma_H \rho_H \exp(-\sigma_H^2 q^2/2) \cos(qz_i), \tag{11}$$

where $i = a, c$. Again, similar expressions apply for the stroma lamellae.

APPENDIX C
Density adjustment

The particle density per layer in the grana, ρ_G, is the ratio of the number of particles per layer, N_{layer}, and the disc area, *i.e.*

$$\rho_G = \frac{N_{layer}}{\pi R_{inner}^2}, \tag{12}$$

where R_{inner} is the grana radius. The stroma particle density ρ_S is the total stroma particle number N_{stroma} divided by the area A of a one-pitch helicoid sheet, also taking into account the number of connection points m and the total pitch number in the stack. We find that

$$\rho_S = \frac{N_{stroma}}{mAN_{pitch}}, \tag{13}$$

where N_{pitch} is the number of pitches in the total height of the stack. The area $A_{surface}$ of a parametrized surface can be calculated independently of the parametrization as

$$A_{surface} = \iint_\Omega (EG - F^2)^{1/2} \, ds \, d\varphi, \tag{14}$$

where E, F, G are the coefficients of the first fundamental form of the surface (Pressley, 2001). For a helicoid these are given by

$$E = 1, \tag{15}$$

$$F = 0, \tag{16}$$

$$G = s^2 + \lambda^2. \tag{17}$$

Inserting these parameters and performing the integral yields

$$
\begin{aligned}
A &= \int_0^{2\pi} \int_{R_{inner}}^{R_{outer}} (s^2 + \lambda^2)^{1/2} \, ds \, d\varphi = 2\pi \int_{R_{inner}}^{R_{outer}} (s^2 + \lambda^2)^{1/2} \, ds \\
&= 2\pi \{ (R_{outer}/2)(R_{outer}^2 + \lambda^2)^{1/2} \\
&\quad + (\lambda^2/2) \ln[R_{outer} + (R_{outer}^2 + \lambda^2)^{1/2}] \} \\
&\quad - 2\pi \{ (R_{inner}/2)(R_{inner}^2 + \lambda^2)^{1/2} \\
&\quad + (\lambda^2/2) \ln[R_{inner} + (R_{inner}^2 + \lambda^2)^{1/2}] \}.
\end{aligned}
\tag{18}
$$

Since $\rho_G/\rho_S = 1$ we find that

$$N_{stroma} = \frac{mAN_{layer}N_{pitch}}{\pi R_{inner}^2}. \tag{19}$$

This then determines the number of particles to simulate in the stroma lamellae, given the dimensions of the system and the number of particles per layer in the grana stack.

References

Blaurock, A. E. (1982). *Biochim. Biophys. Acta*, **650**, 167–207.
Brangeon, J. & Mustardy, L. (1979). *Biol. Cell*. **36**, 71–80.
Brumfeld, V., Charuvi, D., Nevo, R., Chuartzman, S., Tsabari, O., Ohad, I., Shimoni, E. & Reich, Z. (2008). *Plant Cell*, **20**, 2546–2549.
Crist, B. & Morosoff, N. (1973). *J. Polym. Sci.* **11**, 1023–1045.
Förster, S., Timmann, A., Konrad, M., Schellbach, C., Meyer, A., Funari, S. S., Mulvaney, P. & Knott, R. (2005). *J. Phys. Chem. B*, **109**, 1347–1360.
Garab, G. & Mannella, C. A. (2008). *Plant Cell*, **20**, 2549–2551.
Glatter, O. & Kratky, O. (1982). *Small Angle X-ray Scattering*. London: Academic Press.
Gunning, B. E. S. & Steer, M. W. (1975). *Ultrastructure and the Biology of Plant Cells*. London: Edward Arnold Publishers.
Hansen, S. (1990). *J. Appl. Cryst.* **23**, 344–346.
Heinen, U., Poluektov, O., Stavitski, E., Berthold, T., Ohmes, E., Schlesselman, S. L., Golecki, J. R., Moro, G. J., Levanon, H., Thurnauer, M. C. & Kothe, G. (2004). *J. Phys. Chem. B*, **108**, 9498–9504.
Hodapp, N. & Kreutz, W. (1980). *Biochim. Biophys. Acta*, **7**, 65–95.
Holm, J. K. (2004). *Structure and Structural Flexibility of Thylakoid Membranes*. University of Roskilde.
Kirchhoff, H., Mukherjee, U. & Galla, H. J. (2002). *Biochemistry*, **41**, 4872–4882.
Kratky, O. & Stabinger, H. (1984). *Colloid Polym. Sci.* **262**, 345–360.
McAlister, B. C. & Grady, B. P. (1998). *J. Appl. Cryst.* **31**, 594–599.
Murakami, S. & Packer, L. (1970). *J. Cell Biol.* **47**, 332–351.
Mustardy, L., Buttle, K., Steinbach, G. & Garab, G. (2008). *Plant Cell*, **20**, 2552–2557.
Mustardy, L. & Garab, G. (2003). *Trends Plant Sci.* **8**, 117–122.
Nagle, J. F. & Tristram-Nagle, S. (2000). *Biochim. Biophys. Acta*, **1469**, 159–195.
Pabst, G., Koschuch, R., Pozo-Navas, B., Rappolt, M., Lohner, K. & Laggner, P. (2003). *J. Appl. Cryst.* **36**, 1378–1388.
Paolillo, D. J. (1970). *J. Cell Sci.* **6**, 243–255.
Paolillo, D. J., MacKay, N. C. & Graffius, J. R. (1969). *Am. J. Bot.* **56**, 344–347.
Posselt, D., Kirkensgaard, J. J. K., Aagaard, T. H., Holm, J. K., Retfalvi, E., Rosta, L., Kovacs, L. & Garab, G. (2009). In preparation.
Pressley, A. (2001). *Elementary Differential Geometry*. New York: Springer.
Schmidt-Rohr, K. (2007). *J. Appl. Cryst.* **40**, 16–25.
Shibayama, M., Nomura, S., Hashimoto, T. & Thomas, E. L. (1989). *J. Appl. Phys.* **66**, 4188–4197.
Shimoni, E., Rav-Hon, O., Ohad, I., Brumfeld, V. & Reich, Z. (2005). *Plant Cell*, **17**, 2580–2586.
Wiener, M. C., Suter, R. M. & Nagle, J. F. (1989). *Biophys. J.* **55**, 315–325.